J Mater Sci: Mater Med (2010) 21:2067–2078
DOI 10.1007/s10856-010-4082-9

Chemico-physical modifications induced by plasma and ozone sterilizations on shape memory polyurethane foams

Luigi De Nardo · Monica Moscatelli · Federica Silvi · Maria Cristina Tanzi · L'Hocine Yahia · Silvia Farè

Received: 10 December 2009 / Accepted: 6 April 2010 / Published online: 21 April 2010

Abstract Thermally activated shape memory polyurethane foams are promising materials for minimally invasive surgical procedures. Understanding their physical and chemical properties, in vitro response and effects of sterilization is mandatory when evaluating their potential as biomaterials. In this work, we report on the characterization of two Cold Hibernated Elastic Memory (CHEM) foams before and after two novel low-temperature sterilization techniques (plasma and ozone). Foams have different transition temperatures (T_{trans}), as determined by Tanδ peaks in DMA tests, that depend on their chemical composition: both foams possess excellent shape recovery ability (Recovery Rate up to 99%) in conventional shape recovery tests. Plasma sterilization (Sterrad® sterilization system) resulted in a slight increase of open porosity, but no effects on bulk chemical and thermo-mechanical properties were observed. Ozone sterilization had a stronger effect on foams morphology, both in terms of an evident rupture of pore walls and surface oxidation. These modifications affected both thermomechanical and shape recovery behavior. Furthermore, plasma sterilized foams cytocompatibility was investigated with L929 fibroblast cell line in vitro, showing a good adhesion and proliferation, as confirmed by SEM observation and Alamar blue assay. The obtained results contribute to define the role of shape memory foams as biomaterials and open novel questions on the role of sterilization technique effects on cellular solids.

L. De Nardo (✉)
Dipartimento di Chimica, Materiali e Ingegneria Chimica "G. Natta", Politecnico di Milano, Via Mancinelli 7, 20131 Milan, Italy
e-mail: luigi.denardo@polimi.it

M. Moscatelli · F. Silvi · M. C. Tanzi · S. Farè
Biomaterials Laboratory, Bioengineering Department, Politecnico di Milano, Piazza Leonardo Da Vinci 32, Milan, Italy

L'HocineYahia
Institute of Biomedical Engineering, École Polytéchnique de Montréal, Montréal, QC, Canada

1 Introduction

Shape memory materials show the ability to recover a permanent shape from a temporary deformed state when an external stimulus is applied. Temperature variations, chemical gradients or electromagnetic fields [1] can induce material's phase transitions, resulting in a macroscopic shape modification. Among these materials, Shape Memory Alloys (SMAs) have found large application in clinical practice, allowing the design of a number of temporary and permanent devices [2–4]. During the last 20 years, the synthesis and characterization of novel polymeric materials with thermally induced shape memory properties have been reported [5]. In Shape Memory Polymers (SMPs), the transition from temporary to permanent shapes is generally stimulated by an external gradient of temperature, in the range of a specific switching transition temperature (T_{trans}).

Compared to SMAs, SMPs possess several advantages, mainly the ability to recover larger deformations (up to 800%) and a strongly temperature-dependent modulus, with variation of orders of magnitude in a narrow temperature range. Moreover, they have low cost, easy manufacturing and good biocompatibility [6–8]. Furthermore, their physical (e.g. transition temperatures) and mechanical properties can be tailored by small changes in chemical composition and structure [5].

Due to all these advantageous properties, the development of SMPs is actively promoted and their use has been proposed in different technological areas [9–12]. In particular, the activation of shape recovery by body temperature represents a powerful mechanism for medical device design, when using materials with T_{trans} in the range of 37°C. Minimally invasive procedures, for instance, could take advantage from such an approach: the ability to be stretched in a temporary shape, that can substantially differ from the "memorized" permanent shape, enables large compressed devices to be introduced into the body and then be expanded to fit a specific anatomic site. Moreover, taking benefits from strongly temperature-dependent modulus, devices with stiffness variation can be also realized.

For several biomedical devices, sterilization is mandatory and a validation before their clinical use is necessary. A number of sterilization techniques are currently employed and it is important that the applied method does not adversely modify chemical and mechanical properties, as well as functionality and biocompatibility [13]. Traditional techniques have limitations in terms of polymer stability (e.g. γ radiation and heat), treatment time, and patient/operator safety (e.g. Ethylene Oxide). To overcome these limitations, efforts have been made in developing new sterilization technologies. Plasma and ozone sterilizations, for instance, are currently employed in medical centers to decontaminate surgical equipments and devices.

Some recent works have been focused on the effects of novel sterilization techniques on chemico-physical and thermo-mechanical properties of polymers [13–16]. Lerouge et al. [16], for instance, showed surface oxidation in polyurethane catheters and tubing and in polyvinylchloride tubing and films after plasma sterilization. More recent papers have analyzed the effects of such sterilization on SMPs, also finding that it can determine a surface oxidation, although resulting in no evident effects on thermo-mechanical properties but in a reproducible cytotoxic response [13].

However, all these works have been based on the analysis of bulk materials, usually films: cellular solids are currently attracting an increasing interest in biomedical applications, e.g. for scaffolds in tissue engineering applications. Moreover, in the aforementioned works, no evidence of effects on shape memory via shape recovery tests have been produced.

In this work, we report on the effects of plasma and ozone sterilizations on chemico-physical, thermo-mechanical and shape recovery properties of two shape memory polyurethane foams, Cold Hibernated Elastic Memory (CHEM) [17–19]. The in vitro cytotoxicity and cytocompatibility of the two CHEM foams were also preliminary evaluated before and after sterilization, using L929 fibroblasts cells line.

2 Materials and methods

2.1 Materials

Two Cold Hibernated Elastic Material (CHEM) foams were kindly provided by W. Sokolowski from Jet Propulsion Laboratory (Pasadena, CA, USA) and synthesized by Mitsubishi Heavy Industry (Nagoya, JP) [17–19]. CHEM 3520 and CHEM 5520 are poly(ether urethane) foams with nominal glass transition temperatures $T_g = 35$°C (in the following C3520) and $T_g = 55$°C (C5520), respectively. Cylindrical specimens ($\Phi = 15$ mm) were punched from foam slices (h = 10 mm) by mean of a mechanical die. The obtained cylindrical specimens were used for further characterization, if not otherwise specified.

2.2 Plasma and ozone sterilization

Specimens were subjected either to Plasma (PL) or Ozone (OZ) sterilization, according to indications of the manufacturer sterilization system.

Foam specimens underwent plasma sterilization in a Sterrad® system (100S, Johnson & Johnson) according to standard manufacturer procedures and clinical practice (Istituto Nazionale per lo Studio e la Cura dei Tumori (Milan, Italy)): a 400 W radio-frequency power (RF, 13.56 MHz) is applied at a pressure of 500 mTorr (67 Pa), after injection of vaporized H_2O_2, to generate the plasma phase. The overall plasma sterilization cycle is about 52 min and it is performed at room temperature: more details about this treatment in terms of temperature, pressure and system configuration can be found in [20].

Ozone sterilization was performed by using a TSO3 system (125L, TSO3 Inc. Québec, QC, Canada) at Institut de Cardiologie de Montréal (Montréal, QC, Canada). In this system, medical quality oxygen is released into the ozone-generating unit and then subjected to an electrical field, which converts the oxygen into ozone. The ozone is then fed into a humidified sterilization chamber and is subsequently reverted into oxygen using an ozone converting catalyst. The only residues left at the end of the sterilization cycle are oxygen and clean water vapor [21]. The process time is about 4 h 30′ at T = 31 – 36°C.

2.3 Morphological analysis

Specimens were submitted to morphological evaluation by a Scanning Electron Microscope (SEM EVO50EP, Zeiss) at 7.5–10 kV and working distance 10–18 mm, coupled with an Energy Dispersion X-Ray Spectroscopy for surface microanalyses (EDS, Oxford INCA 200).

2.4 Chemico-physical characterization

Foam density was evaluated according to the standard practice EN ISO 845: after conditioning for 24 h at 25°C, specimens ($n = 12$ for each CHEM foam) were weighed and measured.

IR spectra were recorded using a Nicolet FTIR 6700 spectrometer (Thermo Electron Co.) in ATR mode using an ATR Single Bounce accessory and ZnSe crystal. Samples were clamped onto the ZnSe crystal by the standard pressure device tip (2 mm diameter), which defines the effective spot size. Three different points were chosen for each sample (1–3 mm thick) to verify the homogeneity of the chemical modifications occurring upon sterilization. Peak height analysis was performed on bands listed in Table 1, corresponding to the characteristic absorption frequencies of soft and hard segments, according to refs. [22–24]. All the considered peaks were normalized to the 1591 cm^{-1} band from aromatic ν(C=C)—considered as internal reference—assuming that the aromatic rings of diphenyl methane diisocyanate in the hard segments are not affected by degradation [25, 26]. Hydrogen-bonded and free carbonyl peaks from urethane groups were determined by peak deconvolution of the 1780–1680 cm^{-1} region using the *Peak Fitting Module*® of *Origin*® *v.7* (OriginLab®) software.

CHEM foam samples (18–20 mg, $n = 3$) were incubated at 37°C for time periods ranging from 2 to 10 days in 5 ml of Phosphate Buffered Saline (PBS, pH 7.4) containing 0.02% NaN_3 as bacteriostatic agent. High Performance Liquid Chromatography (HPLC, Bio-Rad with UV Monitor Model 1306) was performed in order to evaluate the possible release of low molecular weight substances from the material after sterilization treatments.

2.5 Thermo-mechanical analysis

Dynamic Mechanical Analysis (DMA) were performed in compression mode at heating rate of 1°C min^{-1} in the temperature range 0–220°C, with an amplitude of 50 μm at 1 Hz (DMA 2980 analyzer, TA Instrument). Storage modulus (E′), Loss modulus (E″) and Tanδ (Tanδ = E″/E′) were recorded: tests were performed in duplicate, according to the standard practice ASTM E1640, using cylindrical specimens (Ø = 10 mm, h = 7 mm).

Table 1 Considered bands for IR peak height analysis

Wavenumber [cm^{-1}]	Assignments
3320	ν(N–H) H bonded
1730	ν(C=O) non-H-bonded carbonyl from urethane
1703	ν(C=O) H-bonded carbonyl from urethane
1591	ν(C=C) benzene ring
1109	ν(C–O–C) ether
1081	ν(C–O–C) CO–O–C from urethane

2.6 Shape memory characterization

Shape memory recovery tests were also performed in compression mode: specimens were heated up to $T_H = T_g + 30$°C and then compressed to $\varepsilon_m = 50\%$. At constant strain (ε_m), each sample was cooled down to $T_L = T_g - 30$°C to fix the temporary shape. At $T = T_L$, stress was released and the sample was allowed to recover to ε_u (ε_u representing the deformation after the stress release and it is a consequence of the fact that resulting temporary shape always differs from the shape achieved by deformation [5]). Specimens were then heated at constant rate ($H_r = 1$°C min^{-1}) to record recovered deformation as a function of temperature or time and the final deformation (ε_p). Strain recovery rate, $R_r(T)$, was then calculated according to the following equation:

$$R_r(T) = \frac{\varepsilon(T) - \varepsilon_p}{\varepsilon_m} \quad (1)$$

and hence plotted versus temperature (T).

2.7 In vitro cytotoxicity tests

In vitro cytotoxicity of the extracts was assessed using L929 murine fibroblasts cells line (ECACC No. 85011425). Extracts were obtained according to the standard practice ASTM F619. Foam samples (Ø = 6 mm, h = 3 mm) were disinfected in 70% v/v ethanol solution followed by UV light exposure (10 min for each side), and then rinsed in sterile PBS. Three samples for each foam were immersed in Dulbecco's Modified Eagle's Medium (DMEM) with 10% Fetal Bovine Serum (FBS) and 1% penicillin/streptomycin, maintaining a ratio material/medium of 0.04 cm^3 ml^{-1}. After 2 and 7 days of incubation, medium extracts were put in contact with L929 cells (cell density = 1×10^5 cells ml^{-1}) in 96-well tissue culture plates (TCPS) up to 48 h. Cell viability was evaluated by MTT-biochemical assay (3-(4,5-Dimethylthiazol-2-yl)-2,5-diphenyltetrazolium bromide, a tetrazole). At different timepoints, culture medium was replaced with 200 μl of MTT (Sigma-Aldrich) solution and incubated for 4 h at 37°C and 5% CO_2. Afterwards, MTT solution was replaced with 200 μl of DMSO (Merk) and the multiwell plate was shaken until complete salt crystal dissolution. Absorbance was measured using a Tecan Genius Plus plate reader. Measured absorbance was expressed as relative ratio over control cells on TCPs in 2 and 7 days extracts.

2.8 In vitro cytocompatibility tests

In vitro cytocompatibility of CHEM foams was also assessed using L929 cells. L929 cells were suspended in DMEM culture medium at the density of 7.5×10^5 cell ml^{-1}. The cell suspension (100 µl/well) was seeded onto each CHEM foam specimen, placed in a 96-multiwell culture plate and cultured in an incubator (5% CO_2, 37°C) up to 7 days. Cells viability was assessed using Alamar Blue colorimetric assay. At each time point, the culture medium was replaced with 1 ml Alamar Blue™ (Serotec) solution (10% v/v in culture medium) and the plate incubated for 4 h. 100 µl (3 replicates for each sample) of the surrounding medium was removed from each well, transferred to a 96 well plate and the absorbance measured using a Tecan Genius Plus plate reader. Samples were subsequently rinsed with PBS, fresh culture medium was then added to each well and the plate was returned to the incubator. To evaluate cell morphology, at each timepoint (3 h, 1, 3 and 7 days after seeding), CHEM foams specimens ($n = 2$ for each time point) were fixed with 1.5% v/v glutaraldehyde solution buffered in 0.1 M sodium cacodylate (pH 7.2), dehydrated through a series of ethyl alcohol solutions (20% to 100% v/v ethyl alcohol in distilled water) and then air dried. Specimens were gold-sputtered (Edwards S150B, operating at 0.2 mbar, 1 kV, 20 mA for 1 min) and examined by SEM (SEM EVO50EP, Zeiss) at an accelerating voltage of 7.5 kV and working distance 7–9 mm.

2.9 Statistical analysis

Statistical analysis (Origin 7.0 software) were performed using a *t*-test (student test), with significance level $P = 0.05$. Before each statistical test, normal distribution was verified by normal probability plots.

3 Results

3.1 Effects of plasma and ozone sterilization

3.1.1 Morphological properties

SEM micrographs of both C3520 and C5520 polyurethane foams, before and after plasma and ozone sterilizations, are reported in Fig. 1. C3520 foams (Fig. 1a) show a uniform porosity in terms of dimension distribution: pores have regular spherical shape and show low interconnection. C5520 foams (Fig. 1d) have a morphology similar to C3520, characterized by a higher pore interconnection. Moreover, pores of C3520 foams have an average diameter lower than C5520 ($\Phi = 375$ µm vs. $\Phi = 419$ µm for CHEM 3520 and CHEM 5520 foams, respectively). Observed lacerations on CHEM 5520 surface (Fig. 1d) are probably due to specimen cutting procedure.

SEM images of plasma sterilized foams show a general increase of interconnections between the pores (Fig. 1b, e). In C3520PL and C5520PL foams pore wall ruptures have been observed. Ozone sterilization resulted in a more evident morphological effect: both C3520OZ and C5520OZ foams (Fig. 1c, f) show a greater pore interconnection, when compared to both control and plasma sterilized foams. Moreover, at higher magnification, submicrometric cracks have also been detected on the C3520OZ foams. Finally, C5520OZ (Fig. 1f) shows more irregular profiles of interconnected pores, even if no cracks have been observed on their pore walls.

Densities of C3520 and C5520 foams before and after sterilizations are reported in Table 2: density decrease after plasma sterilization is not statistically significant ($P > 0.05$), whereas following ozone sterilization process, only C3520 foam density significantly decreased ($P < 0.05$).

3.1.2 Chemical properties

ATR-FT IR spectra show the same peaks for both C3520 and C5520 foams, indicating no differences in chemical composition between the two materials. In particular, 1699 cm^{-1} peak indicates the presence of C=O urethane bonds, 1220 and 1104 cm^{-1} peaks indicate, respectively, the presence of C–O and C–O–C bonds and they are characteristic for poly(ether urethane)s (spectra not shown). After plasma and ozone sterilization treatments, the presence of new bands was not detected.

To investigate possible change in phase separation onto the surface of CHEM samples after sterilization, peak height analysis was performed. Table 3 shows the obtained IR peak ratios and their percent variations after plasma and ozone sterilization. After plasma treatment, the peak height ratios related to both hard (3320, 1730, 1703, and 1081 cm^{-1}) and soft segments (1109 cm^{-1}) showed a slight and uniform increase (<5%). Because the ratio between non-hydrogen-bonded and free urethane carbonyls was unchanged vs. control (i.e., $H_{1730}/H_{1703} = 0.5$ and 0.4, respectively for 3520 and 5520), it can be assumed that the surface degradation was homogeneous.

Conversely, ozone sterilization caused a noticeable change in all the considered peak ratios, related to both hard and soft segments. The increase in H-bonded NH and urethane carbonyls, together with a decrease of non-hydrogen-bonded carbonyls, indicates a more extended phase separation on these samples, with rearrangement of hydrogen bonds.

HPLC chromatograms for extracts at 2, 7 and 10 days for C3520, C3520PL, C5520, and C5520PL foams shows the characteristic peak of phosphate buffered saline (PBS)

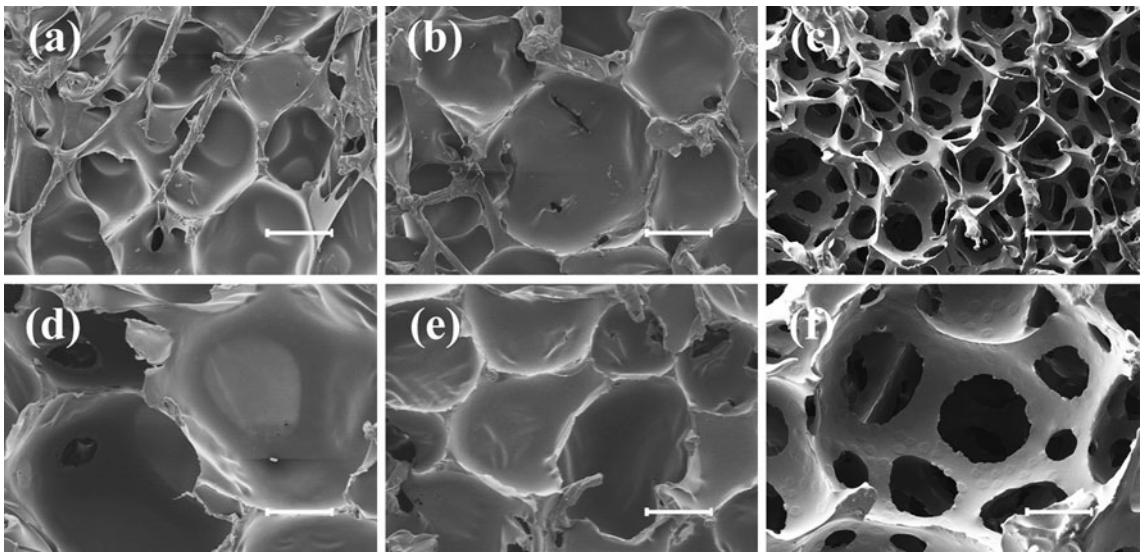

Fig. 1 SEM micrographs of CHEM polyurethane foams: **a** C3520, **b** C3520PL, **c** C3520OZ, **d** C5520, **e** C5520PL, **f** C5520OZ (*Scale bar* 200 μm)

Table 2 C3520 and C5520 foams untreated (CO), Plasma (PL), and Ozone sterilized (OZ): density and transition temperatures from DMA analysis

	Density (S.D.) (g cm^{-3})	Tg (°C)	Tm (°C)	T_{MAX} (dRr/dT) (°C)
C3520	0.121(0.003)	32.2	129.6	29.9
C3520PL	0.127(0.003)	32.3	117.2	31.6
C3520OZ	0.114(0.003)	23.1	109.0	25.0
C5520	0.113(0.007)	45.1	158.0	58.3
C5520PL	0.105(0.004)	49.0	137.0	67.2
C5520OZ	0.107(0.006)	39.6	135.2	52.0

Table 3 ATR-FTIR peak height deconvolution analysis results (in round brackets, percentage variations *vs*. reference peak of control foams)

Material	H_{3320}/H_{1591}	H_{1730}/H_{1591}	H_{1708}/H_{1591}	H_{1109}/H_{1591}	H_{1081}/H_{1591}
C3520	0.44 ± 0.01	0.88 ± 0.06	1.86 ± 0.03	1.75 ± 0.02	2.52 ± 0.07
C3520PL	0.47 ± 0.02 (+5)	0.90 ± 0.08 (+2)	1.93 ± 0.06 (+4)	1.77 ± 0.05 (+1)	2.54 ± 0.08 (+1)
C3520OZ	0.83 ± 0.09 (+88)	0.53 ± 0.15 (−40)	2.43 ± 0.13 (+31)	1.80 ± 0.26 (+3)	2.73 ± 0.35 (+8)
C5520	0.53 ± 0.01	0.75 ± 0.05	1.94 ± 0.05	1.44 ± 0.01	2.27 ± 0.07
C5520PL	0.54 ± 0.04 (+2)	0.76 ± 0.06 (+1)	1.96 ± 0.15 (+1)	1.40 ± 0.08 (−3)	2.20 ± 0.11 (−3)
C5520OZ	0.69 ± 0.16 (+31)	0.59 ± 0.34 (−22)	2.41 ± 0.13 (+24)	2.21 ± 0.24 (+53)	3.57 ± 0.32 (+57)

solution, with a shoulder determined by the presence of NaN_3. Chromatograms of ozone sterilized foams, C3520OZ and C5520OZ specimens, at each timepoint (2, 7 and 10 days), showed a second peak at 20 min, being an indication of possible low molecular weight products release (data not shown).

3.1.3 Dynamic mechanical properties

Results of dynamic mechanical analysis for C3520 and C5520, before and after sterilization, are reported in Figs. 2 and 3, respectively. Transition temperatures obtained from the analysis of storage modulus (E′) and Tanδ are summarized in Table 2.

Figure 2a shows the C3520 storage modulus and Tanδ temperature dependence: a decrease of two orders of magnitude in E′ is evident, as a consequence of the transition from the glassy to rubbery state. The onset temperature of this transition is 12°C. At 129.6°C the onset of a second transition temperature can be observed, due to the melting of the crystalline domains, resulting in a further decrease of E′. Tan δ plot (Fig. 2b) shows a peak at 32.2°C,

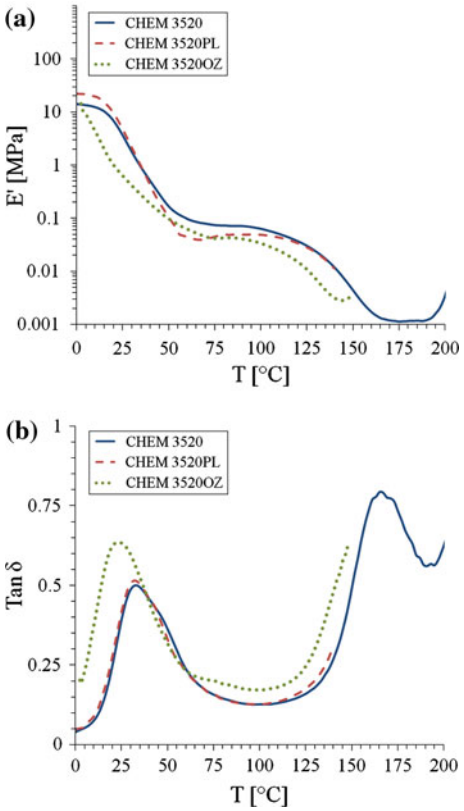

Fig. 2 Dynamic Mechanical Analysis of CHEM 3520 control (C3520), plasma sterilized (C3520PL), and ozone sterilized (C3520OZ): **a** Storage Modulus and **b** Tan delta vs. temperature

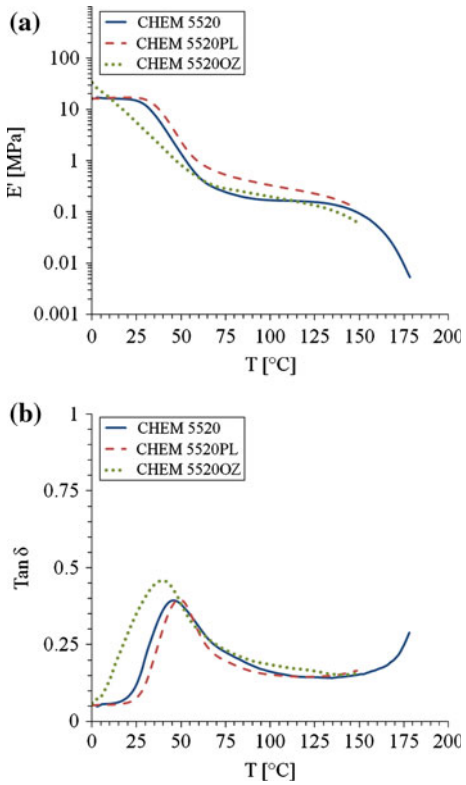

Fig. 3 Dynamic Mechanical Analysis of CHEM 5520 control (C5520), plasma sterilized (C5520PL), and ozone sterilized (C5520OZ): **a** Storage Modulus and **b** Tan delta vs. temperature

that represents the material T_g, that corresponds to T_{trans} activating the shape memory effect. Plasma sterilization seems to have a slight effects on dynamic mechanical properties as well as on transition temperatures: both E′ and Tanδ plots of C3520PL are comparable to those obtained for C3520. E' and Tanδ plots for C3520OZ specimens evidenced a significant effect on thermo-mechanical properties induced by ozone sterilization (Fig. 2a, b). Two main effects are noticed: a downshift of T_g and the rubbery plateau temperature range decrease. The negative shift of T_{trans} is evident from the analysis of Tanδ behavior, that shows a peak at 23.1°C. E′ glassy transition onset has not clearly identified, due to the wider temperature range of transition from glassy to rubbery state. Moreover, a downshift of melting temperature E′ onset after ozone sterilization at 96°C is evident (vs. 129.6°C for C3520 specimens).

Figure 3 shows the temperature dependence of storage modulus and Tanδ for C5520. As expected, T_g of C5520 foam is higher than C3520, even if CHEM 5520 foam exhibit a difference between the T_g and nominal value (Table 2). E′ onset temperature, from glassy to rubbery state, can be observed at 29.5°C and Tanδ peak at 45.1°C. Effects of plasma sterilization on C5520 are negligible (Tanδ peak at 49°C), while a significant effect of the ozone sterilization was evidenced (Tanδ peak at 39.6°C), once again with a downshift of T_{trans}.

3.1.4 Shape memory recovery

Results of shape memory recovery tests on specimens before and after plasma and ozone sterilization are reported in Fig. 4. For both foams, high final shape recovery rate values (R_r) were found, as well as high shape retention during the programming of the temporary shape.

The results of shape recovery tests on C3520, C3520PL and C3520OZ foams are reported in Fig. 4a. As for DMA analysis results, no evident differences between control and plasma sterilized specimens can be noticed. Conversely, C3520OZ specimens show a different behavior: shape recovery begin at 12°C, reaching a $R_r = 98\%$ at 73°C. For higher temperatures, the recovery decreased, resulting in a R_r lower than 94% at 100°C.

The recovery of C5520 foams begin near 30°C and at 100°C reaches a value of about 90% (Fig. 4b). In this case, the behavior of recovery curve for ozone sterilized foams is similar to both control and plasma sterilized specimens. However, in this case, also the final R_r was slightly lower (83 vs. 89%).

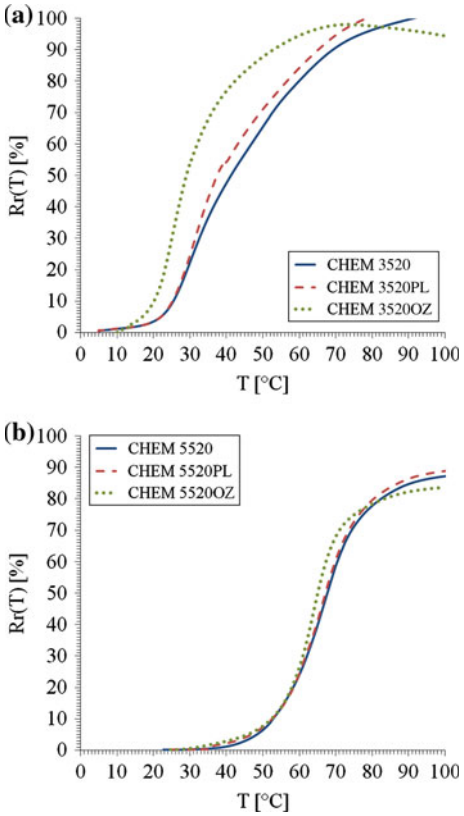

Fig. 4 Shape memory behaviour of control, plasma sterilized (PL), and ozone sterilized (OZ) foams: **a** C3520 and **b** C5520 foams

From the analysis of the dR_r/dT plots (not shown), both C3520 and C3520PL specimens showed a maximum near 32°C, while C3520OZ specimens showed a partial maximum peak around 15°C and a larger peak at 25°C, indicating an irregular behavior during shape recovery. Similarly, for C5520OZ a temperature downshift of the dR_r/dT maximum peak has been evidenced.

3.2 L929 fibroblast cell interaction tests

3.2.1 Cytotoxicity tests

In vitro cytotoxicity tests were performed on extracts of DMEM previously in contact with C3520, C3520PL, C5520, and C5520PL foams. These foams have been selected to be submitted to in vitro cells tests since HPLC analysis on ozone sterilized foams showed a release of low molecular weight products together with a strong modification of their color (evident yellowing). Absorbance values of MTT tests resulted in a no significant difference ($P > 0.05$) between control and plasma sterilized CHEM foams, at both time points. For this reason, in vitro cytocompatibility tests were performed only 3520PL and 5520PL foams.

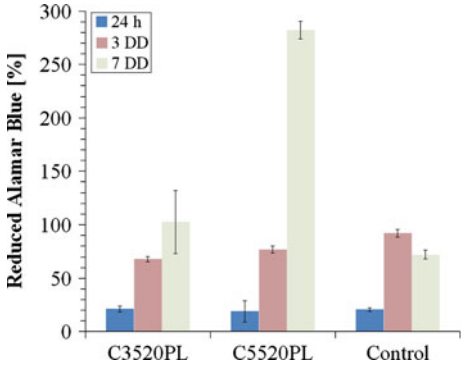

Fig. 5 Alamar Blue test results of in vitro cytocompatibility test on C3520PL and C5520PL foams: absorbance values vs. time

3.2.2 Cytocompatibility tests

Cytocompatibility of C3520PL and C5520PL results of foams evaluated by Reduced Alamar Blue test are shown in Fig. 5 and corresponding SEM micrographs are reported in Figs. 6 and 7 for C3520PL and C5520PL, respectively.

One day after seeding, both foams and TCP (control) showed a similar cells viability; after 3 days, a general increase in the percentage of reduced Alamar Blue can be noticed, indicating an increased cells activity. After 7 days, the viability of cells on C5520PL foams has a value almost four times higher than TCP (control). The values of reduced Alamar Blue increased significantly, compared to 3 days, also for C3520PL (Fig. 5). These results have been confirmed by morphological analysis. In Fig. 6, SEM micrographs at 1, 3 and 7 days on C3520PL are reported: after 1 day (Fig. 6a) few cells can be observed. After 3 days (Fig. 6b) L929 cells begin to spread and colonize foam walls, and a homogeneous distribution of cells on the surface was observed, with a good spreading onto the pore surfaces after 7 days.

For C5520PL, a behavior similar to C3520PL foams can be noticed: after 1 day, L929 cells are few. Some cells are globular, while others started to spread over the surface of the foams. At the second time point (Fig. 7b), more rounded cells can be observed and after 7 days, pore walls appeared completely colonized.

4 Discussion

Polyurethanes are versatile polymeric biomaterials that possess outstanding properties, resulting from their extensive chemico-physical structure diversities. Their bulk and surface properties can be further modulated, without affecting their overall properties, to promote specific biological responses. For instance, suitable drugs, biological factors and functional moieties can be easily incorporated

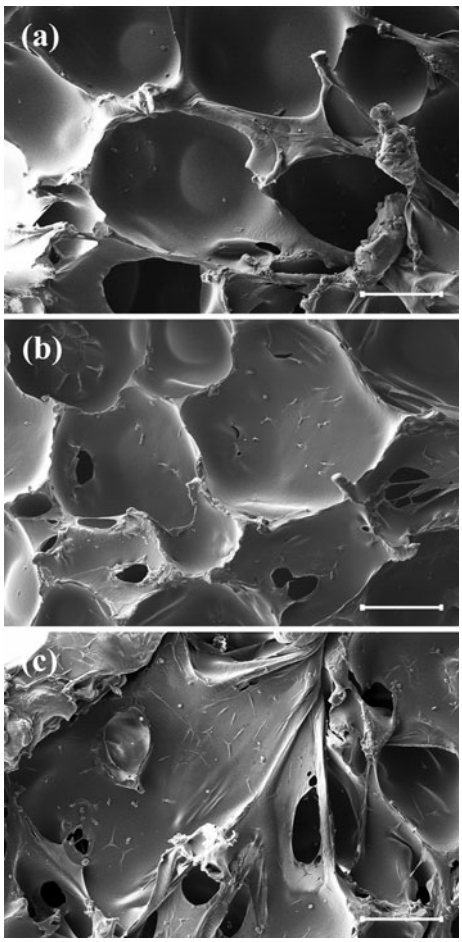

Fig. 6 SEM micrographs of L929 fibroblast cells on Plasma Sterilized C3520 foam: **a** 24 h, **b** 3 days, and **c** 7 days (*Scale bar* 200 μm)

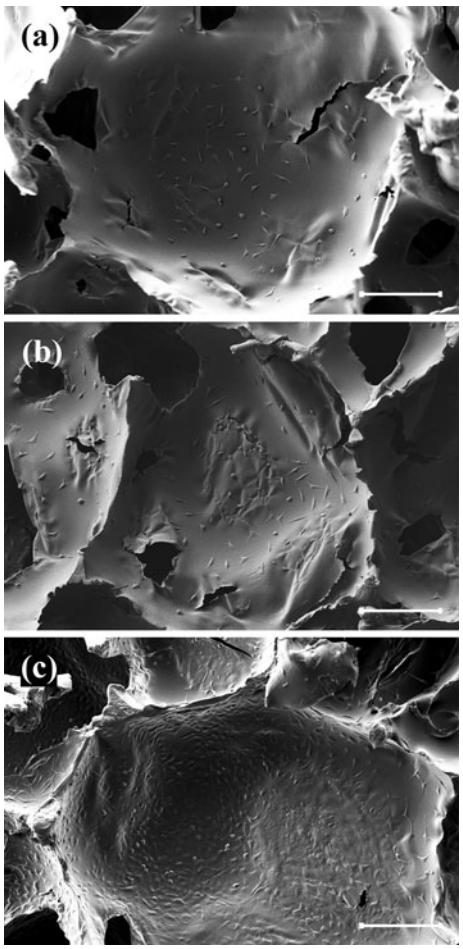

Fig. 7 SEM micrographs of L929 fibroblast cells on Plasma Sterilized C5520 foam: **a** 24 h, **b** 3 days and **c** 7 days (*Scale bar* 200 μm)

in their structure or used for surface functionalization [27]. Such a combination of properties (durability, fatigue resistance, compliance and biocompatibility) allows the design and realization of several temporary disposables and implantable medical devices. Moreover, the development of novel polyurethane chemical formulations, driven by bioengineering design challenges, resulted in a spreading of their applications.

Along this direction, polyurethane-based shape memory polymers have been proposed by several authors [5, 10, 28]: these materials show the ability to recover large deformations when exposed to different external stimuli. Among them, thermally-activated SMPs have several potentials as biomaterials: body temperature could be, in fact, used as natural driving force activating the shape memory behavior. Such an approach makes SMPs ideal candidates for applications in which a temporary shape has to be preserved until the device is locally placed in a specific anatomic site, allowing minimally invasive surgical procedures to be realized by a naturally activated mechanism [6, 7, 12]. Shape memory polyurethane foams could be effectively used, for instance, as occlusive embolization materials because their shape and dimensions can be minimized, allowing minimally invasive surgical procedures. The application of polyurethane foams as embolization material for occlusive procedures was originally proposed by prof. Yahia and coworkers [12, 29]. A similar approach has been also adopted by Maitland and coworkers [30].

As elucidated by Lendlein and Kelch [5], shape-memory technology consists of two main components: (i) the polymer architecture or morphology, that has to fulfil certain structural requirements depending on envisaged applications, and (ii) a special processing and programming technology. Both these points are crucial from a material science point of view, and become critical when SMPs are evaluated as biomaterials. In particular, as suggested by Schoen [31], when developing novel biomaterials and devices, sterilization issues and requirements should be considered at earliest stages of development of a product or material. In this respect, sterilization is not only critical in preventing infections, but also because the selected

technology could permanently modify the surface chemistry or bulk properties of the biomaterial, eventually resulting in an alteration of implant performances. As far as the use of shape memory foams as biomaterial is concerned, this aspect appears of particular importance. SMP foams offer advantageous design tools for innovative devices in medicine, that should not be affected by the selection of the sterilization technique.

As discussed in previous works by ours and several other groups [13, 32, 33], the selection of an appropriate sterilization technique is affected by a variety of parameters. All these works are aimed both at contributing to the development of SMPs application in medicine and understanding the fundamental response of different classes of polymers to conventional and innovative sterilization techniques.

4.1 Effects on chemico-physical properties

Morphological properties of polymer foams depend on their synthesis or transformation process: in CHEM foams, porosity is obtained via an appropriate selection of the blowing agent [17–19]. C3520 and C5520 foams showed a high porosity, resulting in a low density; moreover, an overall low pore interconnection has been evidenced, with similar dimensions and percentage of pores. Plasma and ozone sterilization processes seem to affect the chemico-physical properties of both CHEM foams, even if these properties resulted more severely affected by ozone sterilization, in particular as far as interconnection of pores is concerned.

For plasma sterilization, the increase in pore interconnection should be explained by the fact that foams have been exposed to variable pressures during the sterilization cycle (from atmospheric to 54-67 Pa), vaporized H_2O_2 (at 54 Pa) and low-temperature plasma (400 W RF power) [20]. The cycle is repeated several times: pores have hence been exposed to a negative pressure of approximately 100 kPa, that should have promoted a collapse of thinner pore walls [33]. Interactions with plasma phase are probably limited by the plastic wrapping of the samples [20], whilst the exposure to the chemical agent (H_2O_2), that seems to play a major role in this sterilization system [34], did not affect the surface chemical structure of both CHEM foams.

Ozone sterilization resulted in a more evident modification of the foams morphology. Once again, exposition to cyclic variations of pressure can be one of the main cause of pore interconnection increase. This sterilization technology comprises, in fact, two identical half-cycles, in which vacuum is drawn in the chamber, followed by a humidification step and ozone injection in the chamber [21]. Each cycle is repeated twice, and it is followed by a final ventilation phase to remove ozone from the chamber. A concomitant effect has been played by the presence of ozone, which acts as a strong oxidant for several materials ($O_3 \rightarrow O_2 + O$), in particular for polyurethanes. In fact, ozone-UV sterilization can cause oxidative attack on ether soft segments [35]. It is generally accepted that oxygen centred radicals play an important role as initiators of poly(ether urethanes) oxidation processes and they result in the observed loss of surface ether and surface pitting [36]. In both CHEM foams, a surface oxidation has been observed by ATR-FTIR analysis, evidencing a strong change in soft/hard segments arrangement, compared to the control samples. Surface oxidation is visually confirmed by a strong yellowing of C3520OZ and C5520OZ specimens: photo-activated (UV photons) oxidation mechanisms for aromatic polyurethanes involve the scission of urethane group and oxidation of central methylene group with the formation of a chromophoric reaction product [37].

Exposing polymeric scaffolds to the combined activity of both chemical and physical agents can be critical in terms of resulting modification of material's properties. In this sense, a more pronounced effect after ozone sterilization has been noticed. As this sterilization method appears promising for a practical hospital use, it could be important to set up a specific sterilization procedure for polyurethanes.

4.2 Effects on thermo-mechanical properties

A detailed knowledge of molecular mechanisms of the shape-memory effect and the corresponding structure/property relationship is necessary to understand their mutual dependencies with the aim of effectively drive the design process of novel medical devices. Several authors proposed the use of SMPs in minimally invasive devices design [5, 6, 9–12, 30], as challenging problems correlated to this medical practice should be overcome by the use of this class of materials. The driving idea of using SMPs in less invasive devices is to exploit their ability of having a primary permanent shape that can be recovered from a temporary, smaller one. In thermally activated SMPs, this process is obtained by imposing an external gradient of temperature and a controllable recovery of the primary shape can be hence promoted.

In this work, both C3520 and C5520 foams showed good thermo-mechanical properties, with different transition temperatures. Even if small differences in terms of recovery behaviour has been noticed, as we discussed in a previous work [33], the differences in glass transition temperature affect their selection for medical applications because, at body temperature, the recovery will be different. Differences in glass transition and melting temperatures between the two foams can be correlated to different stoichiometric hard and soft segments ratios [5, 19, 38–40]

in polyurethanes. In fact, isocyanate, polyol and chain extender stochiometry and composition, their relative ratios and polymer process result in a different microstructure.

Plasma sterilization did not seem to affect both thermo-mechanical and shape recovery properties: this result can be considered as a further assessment of the negligible effect of this sterilization on the chemical bulk properties, as previously discussed. Ozone sterilization resulted mainly in a decrease of glass transition temperatures, that affected the shape recovery behaviour as well (effect being more evident in C3520OZ). The different behaviour for CHEM foams after ozone sterilization is strongly related to the increase in phase separation observed by ATR-FTIR analysis. Thermo-mechanical modifications, that have a direct consequence on the shape recovery behaviour, can be both explained by a chemical modification of the materials, as evidenced in the previous section and an alteration of the pore interconnection. The mechanism of linear elasticity, in fact, is strongly influenced on whether the porosity of cellular material is open or closed [41].

4.3 Effects on in vitro cells response

Sterilisation treatments have been proved to adversely affect material properties [13, 16, 20]: any such changes must be fully characterised and accounted for devices being used in applications in which material/cell interactions will take place. Sterilization-induced alterations are generally considered detrimental to the final product in terms of bulk and/or surface properties. However, they may give rise to potentially beneficial changes at a cellular level, with respect to cell/surface interactions [35].

In this work, we investigated both in vitro cytotoxicity and cytocompatibility performances of CHEM foams with L929 cells: biochemical assay confirmed that this material hold a potential for biological tissue interaction with soft tissues. HPLC analysis performed on the extracts showed a low molecular weight products release for both C3520OZ and C5520OZ, confirming an effect on bulk properties induced by this sterilization. For this main reason we decided to no further biologically characterize ozone sterilized foams. Cell proliferation tests, moreover, were conducted only on plasma sterilized foams: if compared with our previously published results [33], material results non cytotoxic and well cytocompatible.

These results are slight different from those obtained in previous published works on different SMPs [13, 32]. Rickert et al. found an increase cell lysis in plasma-sterilized polymer samples after 4 weeks of incubation in MEM, and they provided a possible alteration of the hydrolytic stability combined with an increase in released oligomers as an explanation of this behaviour. In fact, the role played by oligomer alteration and the surface oxidation induced by plasma sterilization is still not enough clear, even if some studies have been carried out on this subject [16].

Yackacki et al. [13] have submitted acrylate-based SMP networks to a variety of sterilization techniques over a broad range of temperatures and methods to choose the optimal conditions. Plasma sterilization (LTP in Yackacki article) was the only method to elicit a severe cytotoxic response, even at short cell test timepoints. Authors explained these results stating that the H_2O_2 vapor phase, that is prevalently responsible for the sterilization in Sterrad systems according to [34], has an affinity toward certain acrylate-based polymers, which can lead to a high enough level of residues and functional groups at the surface to generate a cytotoxic response. Moreover, H_2O_2 molecules react during the plasma process forming ultraviolet photons and hydroxyl radicals (·OH), that graft to and oxidize the surface of the acrylate-based SMP networks [13].

The good preliminary cellular results obtained in this study, compared to the aforementioned works, could be explained according to some main differences due to: (i) different polymeric systems and their consequent different response to the chemico-physical environment generated during the plasma sterilization, (ii) the morphological differences and, (iii) time points selected for testing the cytocompatibility and cytotoxicity.

For all these reasons, it is very important to select the appropriate sterilization method for each type of material, as each polymer has a different structure and components that could be degraded by the sterilizing agent involved in the process.

5 Conclusions

In this work, effects induced by two innovative sterilization techniques on thermally-activated shape memory polymer foams have been investigated, namely plasma and ozone sterilization. Physico-chemical, thermo-mechanical and in vitro cells interaction properties have been evaluated in order to understand the key parameters of this class of cellular solids as possible materials for novel medical device design. Surface morphology has been modified by both sterilization methods, with a more evident increase in pore interconnection for ozone sterilization; such a technique affected in a significant way the chemical structure as well. Thermo-mechanical tests for both CHEM 3520 and 5520 showed a high shape recovery, activated at different T_{trans}, depending on the stochiometric ratio of the foams: both chemical and morphological changes induced by ozone sterilization affected the shape recovery behaviour of this material.

Despite the specific aspects of this work, our results contribute to clarify that the material/device/sterilization have to be taken into account together when innovations in each component of this trio are proposed. These effects should be not necessarily negative: in our case, for instance, plasma sterilization effects have shown interesting results. A slight increase in volume percentage of open cells and the surface modification appear to be a positive factor for the cell colonization, overcoming, for instance, the lack of pore interconnection observed on untreated foams.

Finally, the comparison of the results obtained in this work with previous published researches open new challenges in understanding not only the overall effects of specific sterilization techniques on different shape memory polymers, but also the role of sterilization-induced degradation mechanisms on biological interactions with polymer scaffolds. It is evident that more specific and advanced studies should be carried on, with the aim of contributing to both a correct selection and design of novel biomaterials, for the advanced medical applications requested by the more complex clinical demand.

Acknowledgements Authors would like to thank W. Sokolowski (Jet Propulsion Laboratory, Pasadena, CA, USA) for providing CHEM foams, and Prof. M. Nava (Istituto Nazionale per lo Studio e la Cura dei Tumori, Milan, Italy) for plasma sterilization treatments and Dr. R. Marchand (Montréal, QC, Canada) for Ozone Sterilization. Authors acknowledge Dr. Lorenza Draghi and Dr. Carlo Punta for the useful discussion and text revision.

References

1. Otsuka K, Wayman CM. Shape memory materials. Cambridge: Cambridge University Press; 1998.
2. Gil FJ, Planell JA. Shape memory alloys for medical applications. Proc Inst Mech Eng H J E. 1998;212:473–88.
3. Michiardi A, Aparicio C, Planell JA, Gil FJ. New oxidation treatment of NiTi shape memory alloys to obtain Ni-free surfaces and to improve biocompatibility. J Biomed Mater Res Part B Appl Biomater. 2006;77:249–56.
4. Yahia L'H. Shape memory implants. Hong Kong: Springer; 2000.
5. Lendlein A, Kelch S. Shape-memory polymers. Angew Chem-Int Edit. 2002;41:2034–57.
6. Farè S, De Nardo L, De Cicco S, Jovenitti M, Tanzi MC. Different processing methods to obtain porous structure in shape memory polymers. Mat Sci Forum. 2007;539–543:663–8.
7. Farè S, Valtulina V, Petrini P, Alessandrini E, Pietrocola G, Tanzi MC, Speziale P, Visai L. In vitro interaction of human fibroblasts and platelets with a shape-memory polyurethane. J Biomed Mater Res Part A. 2005;73:1–11.
8. Poilane C, Delobelle P, Lexcellent C, Hayashi S, Tobushi H. Analysis of the mechanical behavior of shape memory polymer membranes by nanoindentation, bulging and point membrane deflection tests. Thin Solid Films. 2000;379:156–65.
9. Lendlein A, Kelch S. Degradable, multifunctional polymeric biomaterials with shape-memory. Mat Sci Forum. 2005;492–493:219–24.
10. Lendlein A, Kratz K, Kelch S. Smart implant materials. Med Device Technol. 2005;16:12–4.
11. Lendlein A, Langer R. Biodegradable, elastic shape-memory polymers for potential biomedical applications. Science. 2002;296:1673–6.
12. Metcalfe A, Desfaits AC, Salazkin I, Yahia L, Sokolowski WM, Raymond J. Cold hibernated elastic memory foams for endovascular interventions. Biomaterials. 2003;24:491–7.
13. Yakacki CM, Lyons MB, Rech B, Gall K, Shandas R. Cytotoxicity and thermomechanical behavior of biomedical shape-memory polymer networks post-sterilization. Biomed Mater. 2008;3:15010.
14. Lee K, Paek KH, Ju WT, Lee Y. Sterilization of bacteria, yeast, and bacterial endospores by atmospheric-pressure cold plasma using helium and oxygen. J Microbiol. 2006;44:269–75.
15. Moisan M, Barbeau J, Moreau S, Pelletier J, Tabrizian M, Yahia LH. Low-temperature sterilization using gas plasmas: a review of the experiments and an analysis of the inactivation mechanisms. Int J Pharm. 2001;226:1–21.
16. Lerouge S, Tabrizian M, Wertheimer MR, Marchand R, Yahia L. Safety of plasma-based sterilization: surface modifications of polymeric medical devices induced by Sterrad and Plazlyte processes. Bio-Med Mater Eng. 2002;12:3–13.
17. Sokolowski WM. Cold hibernated elastic memory self-deployable and rigidizable structure and method therefor. Patent US6,702,976; 2004.
18. Sokolowski WM, Chmielewski AB, Hayashi S, Yamada T. Cold hibernated elastic memory (CHEM) self-deployable structures. Proc SPIE Int Soc Opt Eng. 1999;3669:179–85.
19. Hayashi S, Fujimura H. Shape memory polymer foam. Patent US5049591; 1991.
20. Lerouge S, Wertheimer MR, Yahia LH. Plasma sterilization: a review of parameters, mechanisms, and limitations. Plasmas Polym. 2001;6:175–88.
21. Dufresne S, Leblond H, Chaunet M. Relationship between lumen diameter and length sterilized in the 125L ozone sterilizer. Am J Infect Control. 2008;36:291–7.
22. Wu Y, Sellitti C, Anderson JM, Hiltner A, Lodoen GA, Payet CR. An FTIR-ATR investigation of in vivo poly(ether urethane) degradation. J Appl Polym Sci. 1992;46:201–11.
23. Meijs GF, McCarthy SJ, Rizzardo E, Chen YC, Chatelier RC, Brandwood A, Schindhelm K. Degradation of medical-grade polyurethane elastomers—the effect of hydrogen-peroxide in vitro. J Biomed Mater Res. 1993;27:345–56.
24. Farè S, Petrini P, Motta A, Cigada A, Tanzi MC. Synergistic effects of oxidative environments and mechanical stress on in vitro stability of polyetherurethanes and polycarbonateurethanes. J Biomed Mater Res. 1999;45:62–74.
25. Schubert MA, Wiggins MJ, Schaefer MP, Hiltner A, Anderson JM. Oxidative biodegradetion mechanism of biaxially strained poly(etherurethane urea) elastomers. J Biomed Mater Res. 1995;29:337–47.
26. Schubert MA, Wiggins MJ, Anderson JM, Hiltner A. The effect of strain state on the biostability of a poly(etherurethane urea) elastomer. J Biomed Mater Res. 1997;35:319–28.
27. De Nardo L, Farè S, Di Matteo V, Cipolla E, Saino E, Visai L, Speziale P, Tanzi M. New heparinizable modified poly(carbonate urethane) surfaces diminishing bacterial colonization. J Mater Sci Mater M. 2007;18:2109–15.
28. Ward RS. Softenable, shape-memory thermoplastics for biomedical use. Med Device Diagn Ind 1985;24–31.
29. Sokolowski W, Metcalfe A, Hayashi S, Yahia LH, Raymond J. Medical applications of shape memory polymers. Biomed Mater. 2007;2:S23–7.
30. Maitland DJ, Ward SI, Ortega JM, Buckley PR, Rodriguez J, Hartman J, Wilson TS. Prototype laser-activated shape memory

polymer foam device for embolic treatment of aneurysms. J Biomed Opt. 2007;12:030504.
31. Schoen FJ. Introduction. In: Ratner BD, Hoffman AS, Schoen FJ, Lemons JE, editors. Biomaterials science: an introduction to materials in medicine. 2nd ed. San Diego: Elsevier Academic Press; 2004. p. 753–754.
32. Rickert D, Lendlein A, Schmidt M, Kelch S, Roehlke W, Fuhrmann R, Franke RP. In vitro cytotoxicity testing of AB-polymer networks based on oligo(ε-caprolactone) segments after different sterilization techniques. J Biomed Mater Res Part B Appl Biomater. 2003;67B:722–31.
33. De Nardo L, Alberti R, Cigada A, Yahia LH, Tanzi MC, Farè S. Shape memory polymer foams for cerebral aneurysm reparation: effects of plasma sterilization on physical properties and cytocompatibility. Acta Biomater. 2009;5:1508–18.
34. Krebs MC, Becasse P, Verjat D, Darbord JC. Gas-plasma sterilization: relative efficacy of the hydrogen peroxide phase compared with that of the plasma phase. Int J Pharm. 1998;160:75–81.
35. Andrews KD, Hunt JA, Black RA. Effects of sterilisation method on surface topography and in vitro cell behaviour of electrostatically spun scaffolds. Biomaterials. 2007;28:1014–26.
36. Christenson EM, Anderson JM, Hiltner A. Oxidative mechanisms of poly(carbonate urethane) and poly(ether urethane) biodegradation: in vivo and in vitro correlations. J Biomed Mater Res Part A. 2004;70A:245–55.
37. Rosu D, Rosu L, Cascaval CN. IR-change and yellowing of polyurethane as a result of UV irradiation. Polym Degrad Stab. 2009;94:591–6.
38. Hayashi S. Properties and applications of polyurethane-series shape memory polymer. In: Ashida K, Frisch KC, editors. International progress in urethanes. Westport: Technomic Publishing Company; 1993. p. 90–115.
39. Lin JR, Chen LW. Study on shape-memory behavior of polyether-based polyurethanes. I. Influence of the hard-segment content. J Appl Polym Sci. 1998;69:1563–74.
40. Lin JR, Chen LW. Study on shape-memory behavior of polyether-based polyurethanes. II. Influence of soft-segment molecular weight. J Appl Polym Sci. 1998;69:1575–86.
41. Gibson LJ, Ashby MF. The mechanics of foams: basic results. In: Gibson LJ, Ashby MF, editors. Cellular solids. Structure and properties. 1st ed. Oxford: Pergamon Press plc; 1988. p. 120–68.